

Supporting Information

Boron Nitride Nanosheets as Barrier Enhancing Fillers in Melt Processed Composites

*Shaobo Xie, Oana M. Istrate, Peter May, Sebastian Barwich, Alan P. Bell, Umar Khan and Jonathan N. Coleman**

Methods

Transmission electron microscopy (TEM) was performed on a TECNAI G2 20 Twin electron microscope in bright field mode at 200 kV. Ultrathin sections of the films were prepared using a Leica EM UC6 ultramicrotome. The thin sections were collected on 200 mesh copper grids. XRD measurements were performed using a SIEMENS KRISTALLOFLEX – D500 Diffraktometer (40kV, 30mA) with Cu K α radiation (0.154nm) in the 2 θ range from 5 to 60° with a step interval of 0.03°. Differential scanning calorimetry (DSC) analysis was carried out on a Perkin Elmer Diamond differential scanning calorimeter in a nitrogen environment. The film samples (ca. 5 mg) were heated at a rate of 10 °C min⁻¹ from 0 °C to 290 °C, held at 290 °C for 3 min to eliminate the influence of thermal history, and then cooled at a rate of 10 °C min⁻¹ to 0 °C. TGA was performed from room temperature to 900°C on a Perkin-Elmer Pyris 1 TGA Series Apparatus with a heating rate of 10 °C min⁻¹ under air atmosphere. Tensile tests were performed on dumbbell-shaped specimens using a Zwick tensile tester with 25mm gage length, a 100 N load cell and a crosshead speed of 5 mm min⁻¹.

Additional characterisation by TEM, XRD, DSC, TGA and Tensile tests

DSC was used to characterize the thermal behavior of PET and PET/BN composite films. Fig. S1 A shows representing DSC curves during heating scans. The PET samples exhibits a glass transition at ~74°C, a cold crystallization exothermal peak at about 132°C, and a melting endothermal peak at 252.5°C. Figs. S1 B-E show the glass transition temperature (T_g), crystallization temperature (T_C), Cold crystallization temperature (T_{CC}) and crystallinity (X_C) as function of BN loading, respectively. The addition of BNNS did not change the T_g obviously. However T_C of all composites shifted to higher temperatures than for neat PET, and increased with BNNS loading up to 1.0 vol%. T_{CC} of all composites shifted to lower temperatures than for neat PET and decreased with BNNS loading. This suggests that BNNS can nucleate crystallinity for PET. This may be due to the strong interaction between PET molecules and BNNS which may also retard chain mobility and permit PET molecules to cold crystallize or crystallize earlier during heating or cooling, compared with that of neat PET. However the

addition of BNNS did not change crystallinity obviously (Fig. S1 D). The crystallinity of the samples was calculated from

$$X_C = \frac{\Delta H_m - \Delta H_{CC}}{(1-x)\Delta H_m^0}$$

Where ΔH_m is the enthalpy of melting, ΔH_{CC} the enthalpy of cold crystallization, x the BNNS weight fraction and ΔH_m^0 the enthalpy of melting for a 100% crystalline PET, which is taken as 140 J g^{-1} [1].

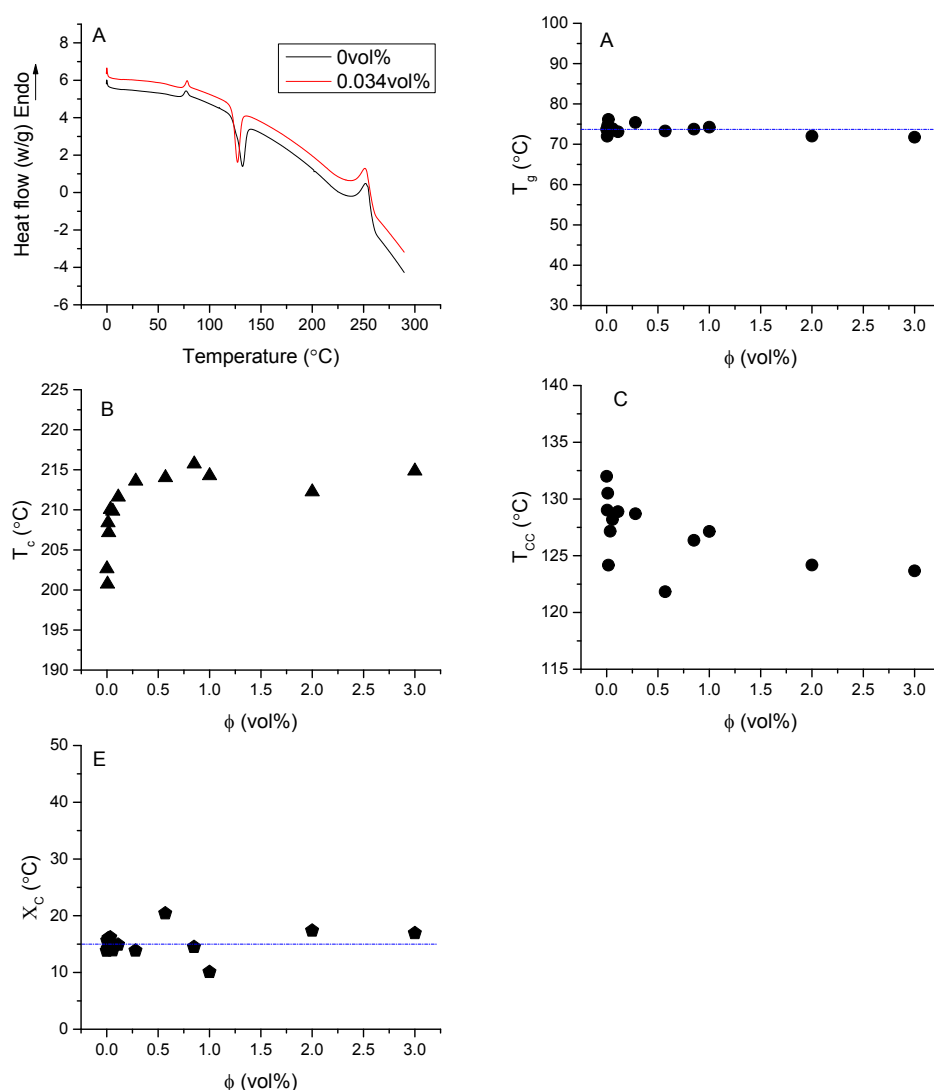


Fig. S1. (A) Representative DSC curves. Thermal properties of PET and PET/BN films as a function of BN loading from DSC measurements: (B) glass transition temperature (T_g); (C) crystallization temperature (T_c); (D) cold crystallization temperature (T_{CC}); (E) crystallinity (X_c).

TGA was used to study the thermal-oxidative stability of PET and PET/BN composite films in air. Fig. S2 A shows representing TGA curves. The presence of BNNS shifted the TGA curves to the higher temperatures, indicating improved thermal-oxidative stability of PET with the addition of BNNS. As shown in Fig. S2 B, the 5% weight loss temperature of all composites shifted to higher temperatures than for neat PET and increased with BNNS loading. A maximum 15°C improvement in $T_{-5\%}$ was found in PET composite with 2.0vol% BN when compared with that of pure PET.

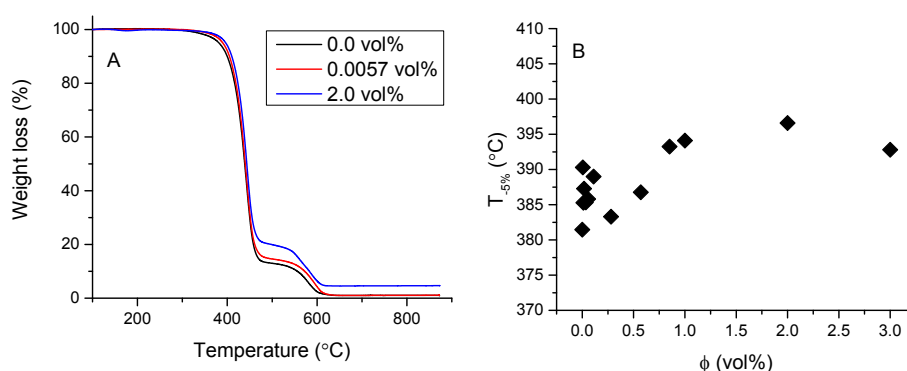


Fig. S2. (A) Representing TGA curves. (B) The 5% weight loss temperature ($T_{-5\%}$) of PET and PET/BN films as a function of BN loading from TGA measurements.

Fig. S3 A shows representing stress-strain curves of PET and PET/BN composites. The tensile mechanical properties of PET and PET/BN composites were summarized in Fig. S3 B-D. All the composites have higher modulus than that of pure PET. We note that at very low volume fractions we see a clear increase in modulus by 25% for a volume fraction of 0.017%. Above this, it falls off, probably due to aggregation. At higher volume fractions, the modulus increases linearly with a slope of $dY/d\phi=25$ GPa, significantly below what would be expected from the rule of mixtures, again due to aggregation effects. The composite with 3.0 vol% BN has the highest modulus, a 53% improvement relative to pure PET. We note that incorporation of just 0.017 vol% BNNS improved the modulus by 27% and improved the strength by 8% relative to pure PET.

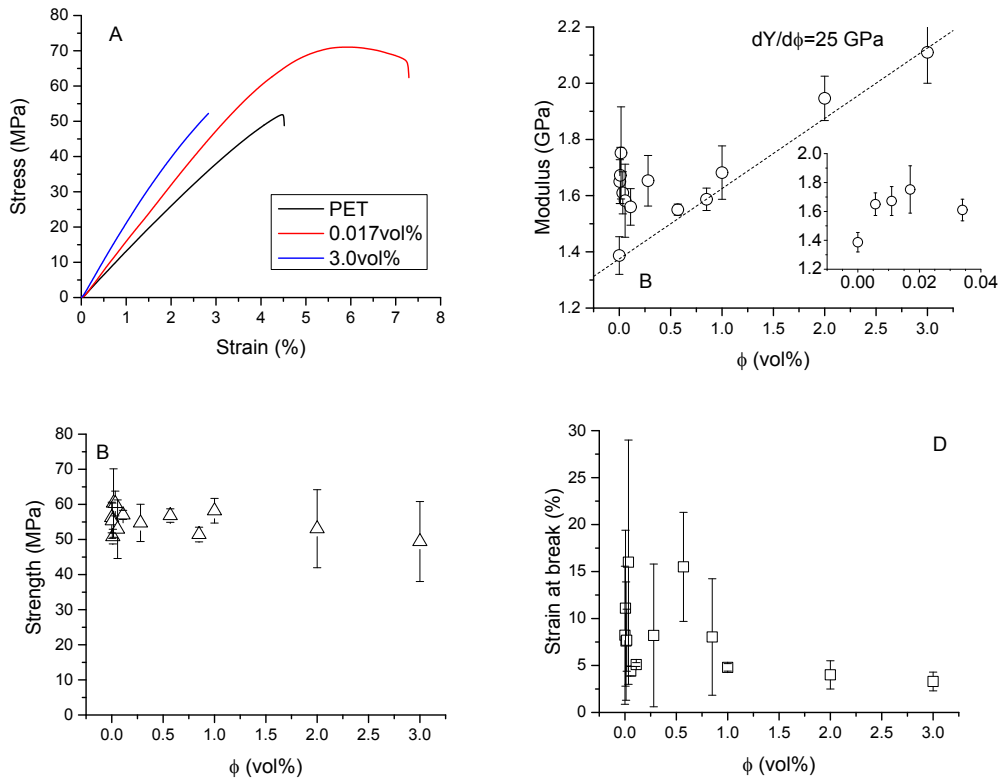


Fig. S3. (A) Representing stress-strain curves of PET and PET/BN composites. Tensile mechanical properties of PET and PET/BN composites as a function of BN loadings: (B) Young's modulus; (C) tensile strength and (D) strain at break.

Fig. S4 shows TEM images of thin ultramicrotomed sections of composite for two BN volume fractions. In most cases, microtoming induced microvoids surrounding the BNNS particles. It also caused the BNNS layers to curve and fold. Unlike HIM, it is relatively difficult to reveal the real dispersion of BNNS in PET matrix by TEM. However, as shown in TEM images, it is clear that at low volume fractions (A), few layer BNNS are not agglomerated and keep their morphological characteristics. However, at higher volume fractions (B) aggregation can be observed.

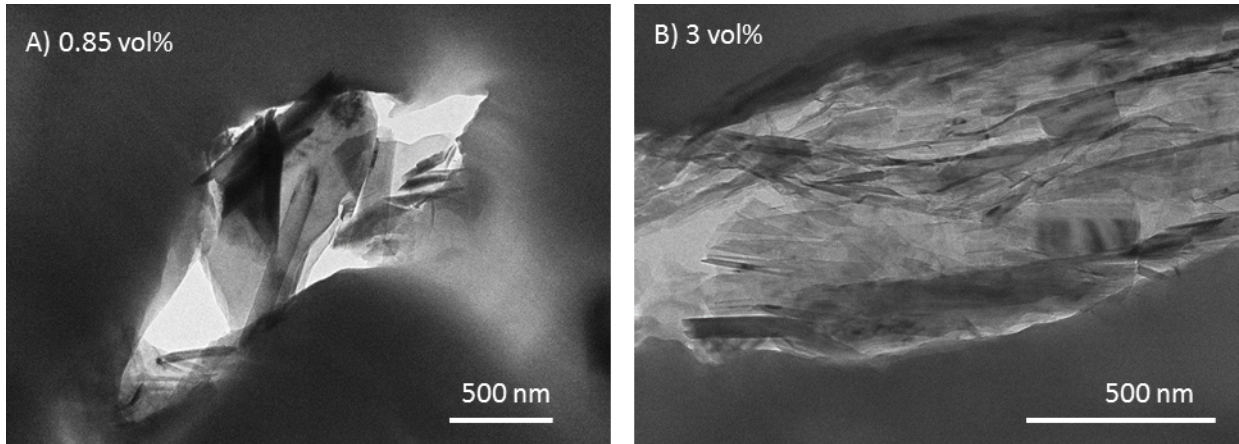


Fig. S4. TEM image representing the dispersion of BNNS in the PET matrix.

Fig. S5 A-B shows the XRD patterns of the as-received raw BN powders and the BNNS made by liquid exfoliation (B is a zoomed graph). The starting BN powders show a typical XRD spectrum of hexagonal BN with strong (002) and (004) peaks at $2\theta=26.81$ and 55.19° respectively. After liquid exfoliation, the relative intensities of the (002) and (004) peaks obviously increase. In contrast, the (100), (101) and (102) peaks at $2\theta=41.66$, 44.03 and 50.21° respectively almost disappear. This is caused by the preferential orientation of the BN platelets on the substrate due to their reduced thickness-to-size ratio by liquid exfoliation. Fig. S5 C shows the XRD patterns of PET and representing PET/BN composite films with BN loading from 0.017 to 3.0 vol%. The (002) peak can only be observed at a BN loading higher than 0.034vol% and its intensities increase with the BN loadings. The (004) peak can be detected at a BN loading higher than 0.57vol%. The disappearing of the (100), (101) and (102) peaks in the whole PET/BN composite films indicates that the well alignment of BNNS in the plane of the films.

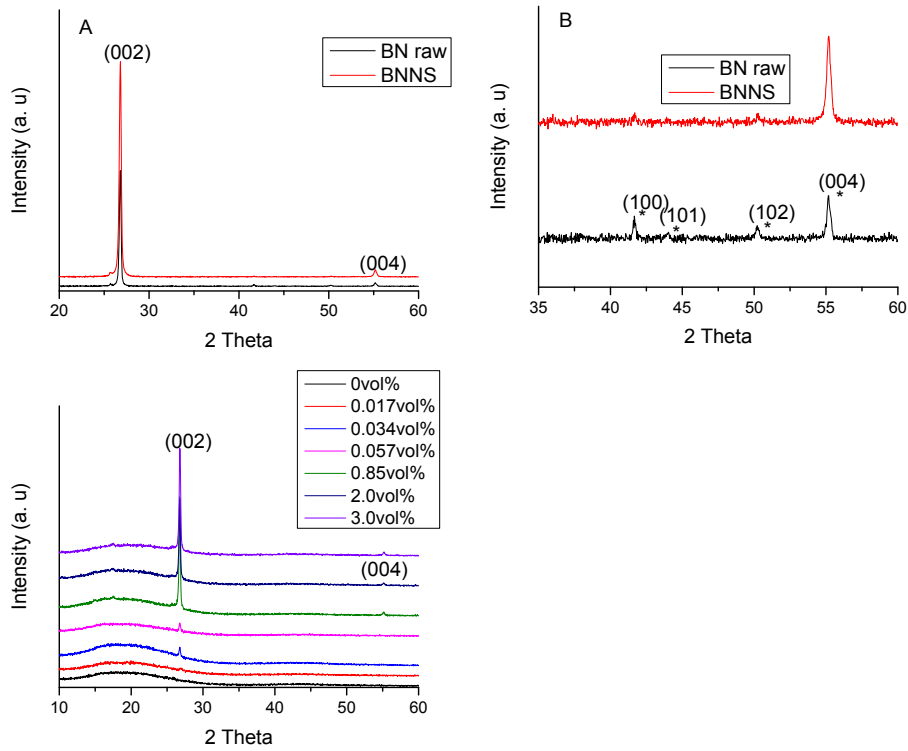


Fig. S5. XRD patterns of the raw BN as received and BNNS made by liquid exfoliation in the 2θ range from 20 to 60° (A) and 30 to 60° (B), and (C) PET and PET/BN films with the indicated BN loading.

References

- [1] Aspy Mehta, Umesh Gaur, Bernhard Wunderlich, Equilibrium melting parameters of poly(ethylene terephthalate). *Journal of Polymer Science: Polymer Physics Edition*, 16, 1978, 289–296.